JOURNAL OF VIROLOGY, Nov. 2006, p. 11370–11380 Vol. 80, No. 22
0022-538X/06/$08.00+0 doi:10.1128/JVI.01041-06

Phospholipase A2 Activity-Dependent Stimulation of Ca^{2+} Entry by Human Parvovirus B19 Capsid Protein VP1▽

Adrian Lupescu,[1]† C.-Thomas Bock,[2]† Philipp A. Lang,[1,2] Susanne Aberle,[2] Heike Kaiser,[2] Reinhard Kandolf,[2] and Florian Lang[1]*

Departments of Physiology[1] and Molecular Pathology,[2] University of Tübingen, Tübingen, Germany

Received 22 May 2006/Accepted 28 August 2006

Recent reports demonstrated an association of human parvovirus B19 with inflammatory cardiomyopathy (iCMP), which is accompanied by endothelial dysfunction. As intracellular Ca^{2+} activity is a key regulator of cell function and participates in mechanisms leading to endothelial dysfunction, the present experiments explored the effects of the B19 capsid proteins VP1 and VP2. A secreted phospholipase A2 (PLA2)-like activity has been located in the VP1 unique region of the B19 minor capsid protein. As PLA2 has recently been shown to activate the store-operated or capacitative Ca^{2+} channel I_{CRAC}, we analyzed the impact of the viral PLA2 motif on Ca^{2+} entry. We cloned the VP1 and VP2 genes isolated from a patient suffering from fatal B19 iCMP into eukaryotic expression vectors. We also generated a B19 replication-competent plasmid to demonstrate PLA2 activity under the control of the complete B19 genome. After the transfection of human endothelial cells (HMEC-1), cytosolic Ca^{2+} activity was determined by utilizing Fura-2 fluorescence. VP1 and VP2 expression did not significantly modify basal cytosolic Ca^{2+} activity or the decline of cytosolic Ca^{2+} activity following the removal of extracellular Ca^{2+}. However, expression of VP1 and of the full-length B19 clone, but not of VP2, significantly accelerated the increase of cytosolic Ca^{2+} activity following the readdition of extracellular Ca^{2+} in the presence of thapsigargin, indicating an activation of I_{CRAC}. The effect of VP1 was mimicked by the PLA2 product lysophosphatidylcholine and abolished by an inactivating mutation of the PLA2-encoding region of the VP1 gene. Our observations point to the activation of Ca^{2+} entry by VP1 PLA2 activity, an effect likely participating in the pathophysiology of B19 infection.

Human parvovirus B19, a nonenveloped virus of about 22 to 24 nm in diameter, is a member of the genus *Erythrovirus* within the family of *Parvoviridae* (35). B19 infection occurs frequently in humans, and this is documented by the high prevalence of specific immunoglobulin G (IgG) antibodies in young children (5% to 15%), adults (60%), and seniors older than 69 years (85%) (15). B19 is the causative agent of erythema infectiosum (fifth disease), hydrops fetalis, and transient aplastic anemia (1, 86). Several studies disclosed an association between B19 and a variety of diseases (43, 48, 63, 80), such as arthritis (56, 77), vasculitic syndromes (19, 24, 31, 80), hepatitis (27, 36, 38, 75, 85), and neurological disorders (2, 85). Specifically, B19 infections have been observed to be associated with acute and chronic myocarditis (13, 16, 30, 44, 53, 58–60, 71). Moreover, the development of endothelial and isolated left ventricle diastolic dysfunction has been associated with B19 infection (81). During pregnancy, parvovirus B19 infection may cause maternal and fetal myocarditis, congenital abnormalities, stillbirth, and abortion (10, 21, 39, 61). The particularly severe course of the antenatal disease may relate to the preference of B19 for proliferating tissues (79).

The cellular receptor for B19 infection has been regarded as a blood group P antigen based on the failure of B19 infection in a patient with a hereditary P antigen defect (12). The P antigen is necessary for B19 binding but not sufficient for virus entry into cells. In this regard, the α5β1 integrin and the recently identified Ku80 autoantigen act as cellular coreceptors for human parvovirus B19 infection (57, 82). Therefore, target cells of B19 are mainly erythroid progenitor cells expressing high levels of P antigen as well as the coreceptors α5β1 integrin and Ku80 autoantigen. However, nonerythroid cell lineages, such as fetal myocytes, follicular dendritic cells, and endothelial cells can be infected by B19 (12, 28, 29, 57, 82). We have recently localized B19 genomes in endothelial cells of myocardial tissue of patients with fatal inflammatory cardiomyopathy, predominantly in small intramyocardial arteries and venoles but not in cardiac myocytes or epicardial coronaries, by using in situ hybridization. Concomitant with endothelial cell infection, marked expression of the adhesion molecule E-selectin, accompanied by margination, adherence, penetration, and perivascular infiltration of the heart by T lymphocytes and macrophages, was noted (17, 42).

The 5.6-kb linear single-stranded DNA genome of B19 contains three large open reading frames (ORFs). The first ORF is located at the 5′ half of the genome and encodes the nonstructural protein NS1, which has a molecular mass of 77 kDa. The NS1 protein represents site-specific DNA binding and is associated with transcriptional and helicase activities (20, 25, 35). The NS1 protein acts as a transactivator on cellular (e.g., interleukin-6) and viral (e.g., human immunodeficiency virus) promoters (54). It has been demonstrated that the cytotoxicity of B19 is closely related to the interference of NS1 with elements of the signaling pathways leading to host cell apoptosis, such as p21/WAF and caspase 3 (37, 55, 76).

* Corresponding author. Mailing address: Physiologisches Institut, der Universität Tübingen, Gmelinstr. 5, D-72076 Tübingen, Germany. Phone: 49 7071 29 72194. Fax: 49 7071 29 5618. E-mail: florian.lang@uni-tuebingen.de.

† A.L. and C.T.B. contributed equally to this study and thus share first authorship.

▽ Published ahead of print on 6 September 2006.

TABLE 1. PCR primer sets used

Primer	Sequence (5′→3′)[a]	Localization (nucleotides) in B19 genome (AF162273)
Primer sets for site-directed mutagenesis		
PVB-^{H153A}VP1 sense	GCT GTT GAC AGT GCT GCA AGG ATT **GC**T GAC TTT AGG TAT AGC CAA CTG GC	3055–3104
PVB-^{H153A}VP1 antisense	GCC AGT TGG CTA TAC CTA AAG TCA **GC**A ATC CTT GCA GCA CTG TCA ACA GC	3055–3104
Primer sets for cloning		
VP1-F	GTA GAT TAT GAG TAA AGA AAG TGG	2616–2639
VP1-R	ACG GTG GGG AGT GTT TAC AAT G	4961–4982
VP2-F	ACC CAA GCA TGA CTT CAG TTA AT	3296–3318
VP2-R	ACG GTG GGG AGT GTT TAC AAT G	4961–4982

[a] Bold letters indicate point mutations.

The second and third ORFs located in the 3′ half of the B19 genome encode the major VP1 and minor VP2 structural capsid proteins (20). VP1 includes a unique sequence of 227 amino acids (VP1u; 84 kDa) and is followed by the entire VP2 sequence (554 amino acids; 58 kDa). Both structural proteins show also a variety of functional activities that are important for the viral life cycle (11, 14, 34). Specifically, a number of amino acids in the highly conserved domain of the VP1u share homologies to the catalytic site and Ca^{2+}-binding loop of secreted phospholipase A2, which has been found in snake and bee venoms (18, 50, 87). A conserved PLA2-like motif (HDXXY) has recently been identified in the N-terminal extension of the VP1 minor capsid protein in approximately 30 different parvoviruses, including B19 (26, 50, 87). The viral Ca^{2+}-dependent PLA2 is supposed to be necessary for viral entry during penetration of endosomal membranes of the host and nuclear targeting of the viral genome, and it may be involved in the synthesis of eicosanoids, which could play an important role in inflammatory reactions and host cell dysfunction (26, 87). It has been shown recently that the B19 PLA2 activity may play a direct role in initiating and accelerating inflammatory processes in synovial tissue by up-regulation of the COX-2 protein (51). In the case of porcine parvovirus (PPV), site-directed mutagenesis of critical amino acids in the catalytic site strongly decreased both the enzyme activity and the virus infectivity (87). This was shown for the mutation at position 153 with a histidine-to-alanine (H153A) exchange which abolishes the enzyme activity of viral PLA2 (vPLA2) (26, 87). When the critical amino acids in the PLA2 active site of the infectious clone of PPV were mutated, virus was still obtained upon transfection but was no longer infectious (87).

Little is known about the mechanisms linking the specific viral proteins to signs and symptoms of parvoviral infection, especially to mechanisms involved in endothelial dysfunction in patients suffering from inflammatory cardiomyopathy. To gain insight into the functional properties of defined parvovirus B19 proteins, we expressed the viral proteins VP1, expressing viral PLA2-like activity, and VP2 in human endothelial cells (HMEC-1) and exerted a B19 infectious clone to demonstrate the PLA2 activity under the control of the complete B19 genome. In order to prove the general importance of the B19 PLA2 enzymatic activity also in cells not permissive for B19, we expressed the VP1, ^{H153A}VP1, and VP2 proteins under the control of a ponasterone A-inducible promoter in 10SW retinoblastoma cells. As cytosolic Ca^{2+} activity is a critical regulator of host cell proliferation and apoptosis (4–6, 62) and as

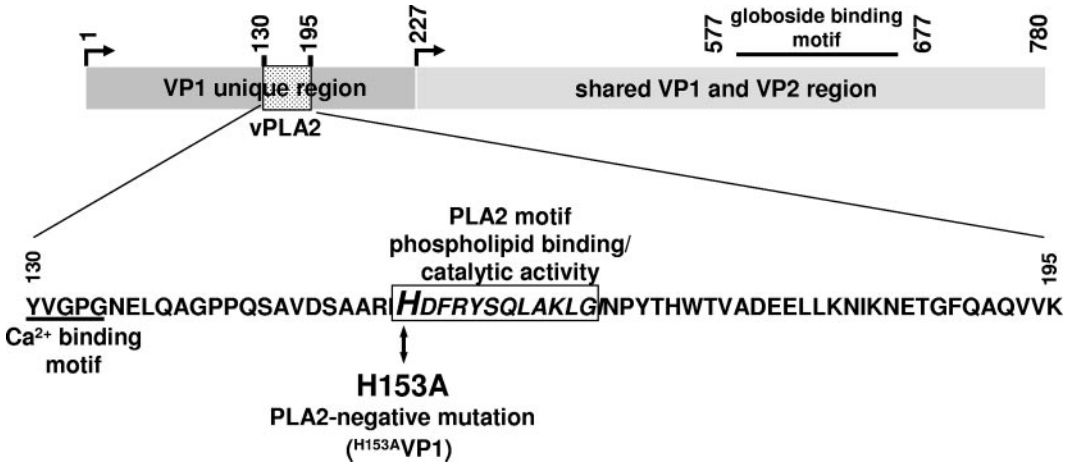

FIG. 1. Schematic presentation of the B19 VP1/VP2-region. The PLA2 motif located in the VP1 unique region is indicated by amino acid sequences. The catalytic site of the PLA2 motif is marked by italic letters. The position of the mutation H153A (for PLA2-negative ^{H153A}VP1) is indicated.

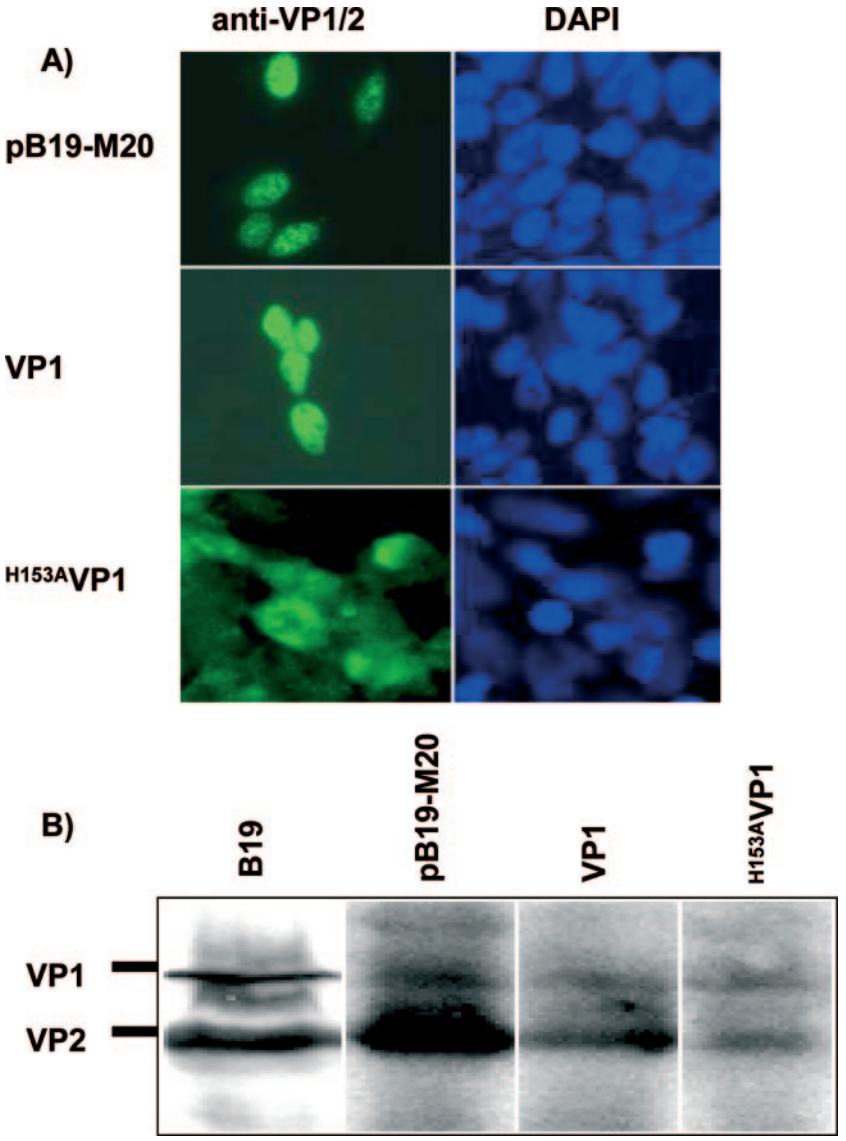

FIG. 2. Expression of VP1 proteins in HMEC-1 cells. Images from immunofluorescence experiments (A) and Western blot analysis (B) of VP1 protein abundance in HMEC-1 cells are shown. (A) Expression of the B19 replication-competent plasmid pB19-M20 (upper panel) and the VP1 (middle panel) and ^{H153A}VP1 (lower panel) proteins in transfected HMEC-1 cells as detected with monoclonal anti-VP2 and secondary FITC-labeled goat anti-mouse antibodies 48 h after transfection. The corresponding images of DAPI staining is shown on the right. (B) Western blots showing expression of VP1 (84 kDa) and VP2 (58 kDa) polypeptides from B19-positive serum, from HMEC-1 cells transfected with pB19-M20, and from pcDNA-VP1 and pcDNA-^{H153A}VP1 constructs. B19-specific VP1/VP2 polypeptides were detected using monoclonal anti-VP2.

mammalian phospholipase A2 has recently been shown to enhance Ca^{2+} entry through the Ca^{2+} release-activated channel I_{CRAC} (74), we searched for their influence on the regulation of cytosolic Ca^{2+} activity.

MATERIALS AND METHODS

Plasmids. B19 DNA (GenBank accession numbers AY768535 and AF162273) was isolated from deparaffinized myocardial tissue of a patient with fatal B19-associated inflammatory cardiomyopathy after proteinase K digestion, phenol-chloroform extraction, and ethanol precipitation. For cloning of the VP1 and VP2 plasmids, the respective regions were amplified by PCR using a high-fidelity polymerase system (Roche, Basel, Switzerland). The primer sets used for the experiments are described in Table 1. The amplicons were digested with the restriction enzymes XbaI and SpeI for VP1 and VP2, respectively, and inserted into the pcDNA 3.1 or pIND vector (Invitrogen, Karlsruhe, Germany). The resulting plasmids pcDNA-VP1, pcDNA-VP2, pIND-VP1, and pIND-VP2 were analyzed by automated DNA sequencing in both directions (BigDye Terminator cycle sequencing kit; PE Applied Biosystems, Foster City, CA) to verify the correct sequences. The replication-competent B19 clone pB19-M20 was a kind gift from K. E. Brown (88). The plasmid pCR-Script (Stratagene, La Jolla, CA) served as a B19-negative control vector for cell culture experiments in which the replication-competent B19 clone pB19-M20 was used.

Site-directed mutagenesis to generate PLA2-negative VP1 protein. To generate a vPLA2-negative VP1 mutant, the amino acid histidine at position 153 of the VP1 unique region was changed to alanine (H153A) (Fig. 1) as previously described for PPV (87) by using site-directed mutagenesis. The point mutation (Table 1) was introduced into the VP1-expressing plasmids pcDNA-VP1 and pIND-VP1. The site-directed mutagenesis was carried out according to the instructions provided with the Quickchange mutagenesis kit by Stratagene (La

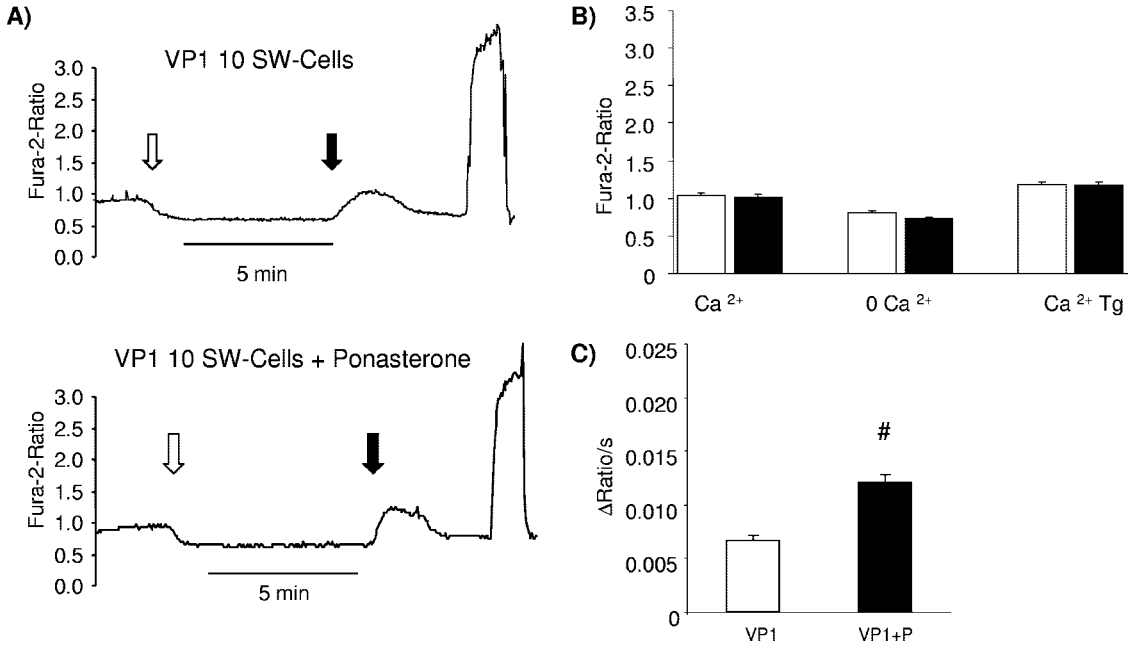

FIG. 3. Increase of Ca^{2+} entry into retinoblastoma cells by expression of VP1. (A) Representative original tracings showing the Fura-2 fluorescence ratios (340/380 nm) in Fura-2-loaded stably transfected VP1-expressing retinoblastoma cells (10SW) exposed initially to Ringer solution containing 1 mM extracellular Ca^{2+} and to nominally Ca^{2+}-free Ringer solution (0 mM Ca^{2+}, 5 mM EGTA; white arrow). During exposure to Ca^{2+}-free solution, Ca^{2+} pump inhibitor thapsigargin (1 μM; Molecular Probes) was added. Subsequently, the cells were exposed to Ringer solution with thapsigargin and Ca^{2+} (black arrow). Finally, the cells were exposed to 10 μM of the Ca^{2+} ionophore ionomycin for calibration in the absence and presence of Ca^{2+}. The upper panel shows results for cells in the absence of ponasterone A, and the lower panel shows results for cells in the presence of ponasterone A for stimulation of the induction of VP1 expression. (B) Arithmetic means (± SEM; n = 10) of the Fura-2 fluorescence ratios after incubation, as described for panel A, in Ca^{2+}-containing extracellular fluid and in Ca^{2+}-free and thapsigargin (Tg)-containing Ringer solution, and following the readdition of extracellular Ca^{2+}. Open bars represent cells in the absence of ponasterone A, and filled bars represent cells in the presence of ponasterone A for the stimulation of VP1 expression. (C) Arithmetic means (± SEM; n = 10) of the slopes of increasing Fura-2 fluorescence ratios (change in ratio/second) after the readdition of Ca^{2+} in cells incubated as described for panel A in the absence and presence of ponasterone A (P). The number sign indicates a significant difference ($P \leq 0.05$, analysis of variance) compared to the respective value for cells in the absence of ponasterone A.

Jolla, CA). Primers (Table 1) for the mutagenesis reaction were synthesized by MWG (Munich, Germany) and purified to 99.9% homogeneity by high-performance liquid chromatography. Mutagenesis reactions resulted in the generation of the VP1-phospholipase A2 mutant that contained the H153A change (^{H153A}VP1). DpnI digestion (New England Biolabs, Neufahrn, Germany) was used to digest methylated input plasmid DNA, leaving the mutagenesis product intact. Top10F′ *Escherichia coli* cells (Invitrogen, Karlsruhe, Germany) were transformed by DNA from mutagenesis reactions by using standard heat shock procedures. Obtained bacterial colonies were screened by PCR using the forward primer VP1-F and VP1-R (Table 1). Colonies that amplified B19 DNA were inoculated into Terrific broth containing 100 μg/ml ampicillin (Sigma Aldrich, Taufkirchen, Germany) and the plasmid DNA extracted using a miniprep kit (QIAprep Spin; QIAGEN, Hilden, Germany). The correctness of the mutant sequences was confirmed by restriction enzyme digestion and automated DNA sequencing in both directions (BigDye Terminator cycle sequencing kit; PE Applied Biosystems, Foster City, CA) to verify sequence integrity of the H153A mutants.

Cell culture and transfection. All cell culture reagents were purchased from Invitrogen (Karlsruhe, Germany). The immortalized human microvascular endothelial cell line-1 (HMEC-1) was kindly supplied from Thomas Wieder (Department of Physiology, University of Tuebingen, Tuebingen, Germany). HMEC-1 cells were grown in Dulbecco's modified Eagle's medium supplemented with 10% (vol/vol) heat-inactivated fetal calf serum, 1% nonessential amino acids, 1% L-glutamine, 5 mM glucose, 100 units/ml penicillin, 100 μg/ml streptomycin, and 10 ng/ml epidermal growth factor (ICN, Costa Mesa, CA). HMEC-1 cells were seeded in 60-mm cell culture dishes at a concentration of 8×10^5 cells/dish. Transient transfection of HMEC-1 cells was carried out with 10 μg per plate of plasmid DNA using Fugene-6 (Roche Diagnostics, Mannheim, Germany) according to the manufacturer's protocol. After 48 h, cells were exposed to Ca^{2+} ions at the indicated concentrations for 12 h. Thereafter, cells were harvested and analyzed for Fura-2 imaging.

Generation of stable B19 protein-expressing cell lines. Stable inducible B19 protein-expressing VgRXR-10SW cell lines were generated by transfection of human retinoblastoma cells (10SW) expressing the heterodimer ecdysone-retinoid X receptor (RXR), with the pIND-VP1, pIND-^{H153A}VP1, and pIND-VP2 plasmids described above. The ecdysone-RXR binds a modified ecdysone response element in the presence of the ligand ponasterone A (Invitrogen, Karlsruhe, Germany). Transfection experiments were performed as described previously (9). The stable integration of genes encoding B19 VP1, ^{H153A}VP1, and VP2 was tested by PCR of genomic DNA after selection of the stable cell clones by using neomycin (G418; Calbiochem, Bad Soden, Germany). The transcript levels achieved were similar to the levels in B19-infected tissue (e.g., cardiac endothelial cells). The stably transfected VgRXR-10SW cells (herein called VP1-10SW, ^{H153A}VP1-10SW, and VP2-10SW) were maintained in Dulbecco's modified Eagle's medium supplemented with 10% (vol/vol) heat-inactivated fetal calf serum, 1% nonessential amino acids, 1% L-glutamine, 5 mM glucose, 100 units/ml penicillin, 100 μg/ml streptomycin, 400 μg/ml zeocin, and 600 μg/ml G418 (Calbiochem, Bad Soden, Germany) in an atmosphere containing 5% CO_2 at 37°C. Human cells were allowed to recover for 16 h after plating before ponasterone A (5 μM) induction. Cells were seeded in six-well tissue culture plates at 5×10^5 cells per well. Forty-eight hours after ponasterone A induction, cells were exposed to Ca^{2+} ions at the indicated concentrations for 12 h and analyzed for Fura-2 imaging.

Detection of B19 VP1/VP2 gene expression by RT-PCR. Expression of B19 VP1/VP2 RNA of transiently transfected HMEC-1 and stable VP1/VP2-10SW cell lines was confirmed using B19 VP2-specific reverse transcription-PCR (RT-PCR). The detection of B19 VP1/VP2 RNA by RT-PCR using primers specific for the VP1/VP2-coding sequence has been described previously (16, 44). Briefly,

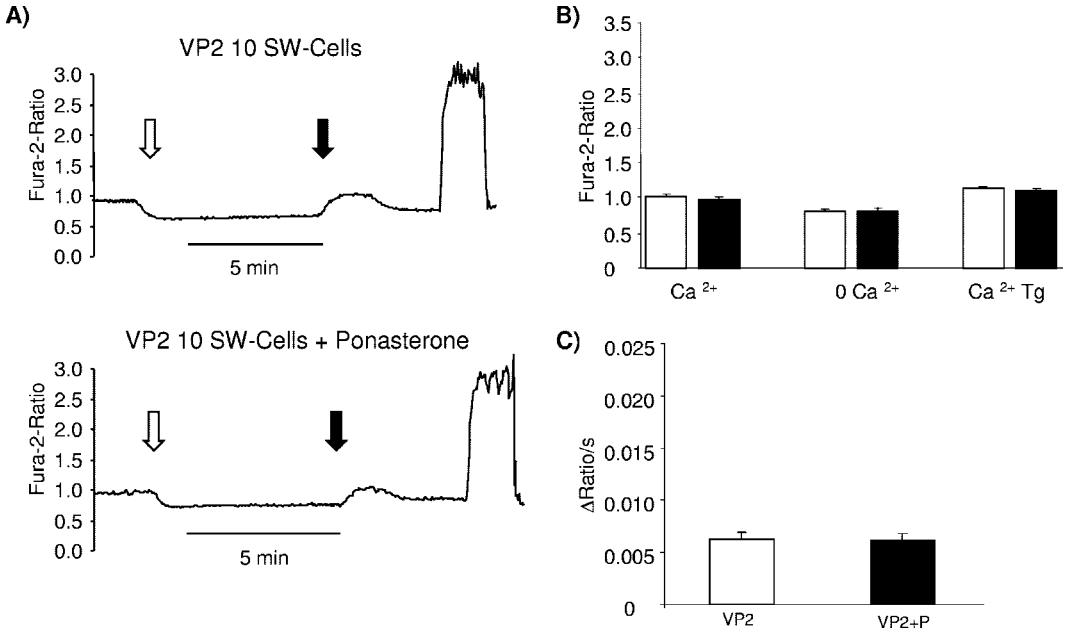

FIG. 4. Lack of effect on cytosolic Ca^{2+} activity by expression of VP2. (A) Representative original tracings showing the Fura-2 fluorescence ratios (340/380 nm) in Fura-2-loaded stably transfected VP2-expressing retinoblastoma cells (10SW) treated as described in the legend to Fig. 3. The upper panel shows results for cells in the absence of ponasterone A, and the lower panel shows results for cells in the presence of ponasterone A. (B) Arithmetic means (± SEM; $n = 8$) of the Fura-2 fluorescence ratios after incubation as described for panel A, in Ca^{2+}-containing extracellular fluid and in Ca^{2+}-free and thapsigargin (Tg)-containing Ringer solution, and following the readdition of extracellular Ca^{2+}. Open bars represent cells in the absence of ponasterone A, and filled bars represent cells in the presence of ponasterone A to stimulate VP2 expression. (C) Arithmetic means (± SEM; $n = 8$) of the slopes of increasing Fura-2 fluorescence ratios (change in ratio/second) after the readdition of Ca^{2+} in cells incubated as described for panel A in the absence and presence of ponasterone A (P).

total RNA (from $\sim 1 \times 10^7$ cells) was extracted using the RNeasy kit (QIAGEN), and first-strand cDNA was synthesized. PCR was performed using primer pairs as described previously (7, 16, 44).

Detection of B19 VP1/VP2 proteins by Western blot analysis. Western blot analysis was performed with whole-cell extracts derived from B19 VP1 transiently transfected HMEC-1 cells and stable VP1-10SW and ^{H153A}VP1-10SW cell lines as described previously (9). B19 VP1/VP2-specific signals were detected using mouse monoclonal anti-VP2 antibodies (clone 521-5D; Chemicon, Planegg-Muenchen, Germany), secondary anti-mouse horseradish peroxidase-fluorescein isothiocyanate (FITC) antibodies (Dianova, Hamburg, Germany) and the ECL detection kit (Applied Biosystems, Darmstadt, Germany) according to the manufacturers' instructions.

Immunofluorescence experiments to detect B19 VP1/VP2 proteins. Immunofluorescence experiments were performed as described previously (9). B19 VP1/VP2 antigen was detected with monoclonal mouse anti-VP2 antibodies (clone R92F6; Chemicon, Planegg-Muenchen, Germany) and anti-mouse FITC-conjugated secondary antibodies (Sigma, Taufkirchen, Germany). Nuclei were stained with 1 g/ml DAPI (4,6-diamidine-2-phenylindole-dihydrochloride; Roche Diagnostics, Mannheim, Germany). Analysis of cells was performed using an immunofluorescence microscope (Zeiss; Oberkochen, Germany).

Solution for cell physiological experiments. Cell physiological experiments were performed at 37°C in Ringer solution containing 125 mM NaCl, 5 mM KCl, 1 mM $MgSO_4$, 32 mM HEPES, 5 mM glucose, and 1 mM $CaCl_2$ (pH 7.4). Where indicated, ionomycin (Sigma, Taufkirchen, Germany) was used at a concentration of 10 μM. The final concentration of the solvent dimethyl sulfoxide was <0.1%.

Measurement of intracellular Ca^{2+}. Fura-2 fluorescence was utilized for cytosolic Ca^{2+} determinations. Intracellular Ca^{2+} measurements were performed as described previously (78). Retinoblastoma cells were loaded with Fura-2 (2.5 μM; Molecular Probes, Goettingen, Germany) for 30 min at 37°C. Fluorescence measurements were carried out with an inverted phase-contrast microscope (Axiovert 100; Zeiss, Oberkochen, Germany). Cells were excited alternatively at 340 and 380 nm, and the light was deflected by a dichroic mirror into the objective (Fluar 40×/1.30 oil; Zeiss, Oberkochen, Germany). Emitted fluorescence intensity was recorded at 505 nm, and data acquisition was performed by using the Imaging Workbench program (Axon Instruments, Foster City, CA). Experiments were made prior to, during, and following exposure to nominally Ca^{2+}-free solution (5 mM EGTA added). In the absence of Ca^{2+}, the intracellular Ca^{2+} stores were depleted by inhibition of the vesicular Ca^{2+} pump by thapsigargin (1 μM; Molecular Probes).

Statistical analysis. Data are expressed as arithmetic means ± standard errors of the means (SEM), and a statistical analysis was done by paired or unpaired *t* test where appropriate.

RESULTS

Cloning and expression of B19 proteins in transient and stably transfected cell lines. In order to determine the effect of the B19 protein VP2 and of the VP1u region, which expresses a phospholipase A2-like activity (26) on the regulation of intracellular Ca^{2+} activity, we amplified the VP1 and VP2 genes from myocardial tissue of a B19-infected patient by PCR. To generate a vPLA2-negative VP1 mutant, the amino acid H153 was changed to A153 (H153A) by using site-directed mutagenesis (Fig. 1). A H153A mutation in the catalytic center of the vPLA2 motif of the VP1u region has previously been described to inhibit vPLA2 enzyme activity in different parvoviruses (26, 51, 87).

The VP1 and VP2 patient-specific PCR products and the ^{H153A}VP1 sequences were introduced into eukaryotic expression vectors (pcDNA and pIND) under the control of a cytomegalovirus promoter or an ecdysone-inducible minimal heat shock promoter, respectively. The pcDNA-VP1 and pcDNA-VP2 constructs and the B19 replication-competent clone pB19-M20 were transiently transfected into HMEC-1 cells. In addition, the retinoblastoma cell line VgRXR-10SW expressing the heterodimer ecdysone-RXR that binds the ecdysone

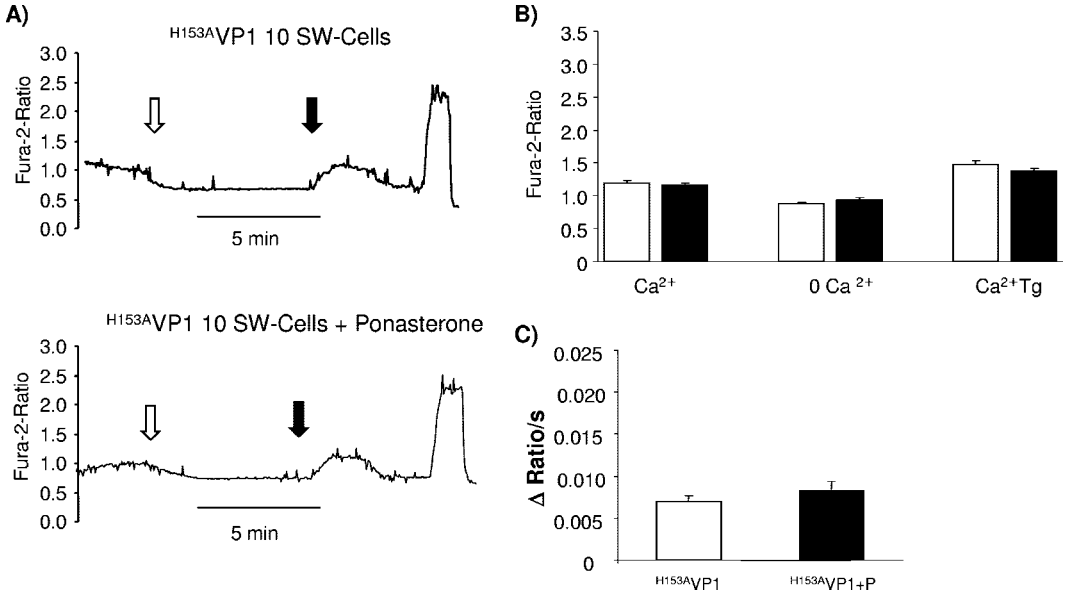

FIG. 5. Lack of effect on cytosolic Ca^{2+} activity by expression of VP1 with inactivated phospholipase A2. (A) Representative original tracings showing the Fura-2 fluorescence ratio (340/380 nm) in Fura-2-loaded stably transfected ^{H153A}VP1 mutant (VP1 PLA2-negative)-expressing retinoblastoma cells (10SW) treated as described in the legend to Fig. 3. The upper panel shows results for cells in the absence of ponasterone A, and the lower panel shows results for cells in the presence of ponasterone A to stimulate ^{H153A}VP1 mutant expression. (B) Arithmetic means (± SEM; $n = 8$) of the Fura-2 fluorescence ratios after incubation as described for panel A, in Ca^{2+}-containing extracellular fluid and in Ca^{2+}-free and thapsigargin (Tg)-containing Ringer solution, and following the readdition of extracellular Ca^{2+}. Open bars represent cells in the absence of ponasterone A, and filled bars represent cells in the presence of ponasterone A. (C) Arithmetic means (± SEM; $n = 8$) of the slopes of increasing Fura-2 fluorescence ratios (change in ratio/second) after the readdition of Ca^{2+} in cells incubated as described for panel A in the absence and presence of ponasterone A (P).

analog ponasterone A was used to generate the stable inducible B19 protein-expressing cell lines VP1-10SW, ^{H153A}VP1-10SW, and VP2-10SW. Upon the addition of ponasterone A, the expression of the B19 proteins was induced. In order to determine the expression of VP1 and ^{H153A}VP1 proteins, RT-PCR (data not shown), immunofluorescence, and Western blot experiments (Fig. 2) were performed. The immunofluorescence experiments showed that VP1/VP2 proteins expressed by the pB19-M20 and pcDNA-VP1 plasmids were mainly located to the cell nuclei (Fig. 2A). This nuclear localization of B19 VP1/VP2 proteins is in good accordance to recently published data (88). However, expression of ^{H153A}VP1 proteins revealed a nuclear and cytoplasmic distribution. The atypical intracellular localization of the mutated protein might be due to the introduced mutation, possibly changing the presentation of putative nuclear localization signals (Fig. 2B). Differences in the amounts of VP1/VP2 proteins detected after transfection of HMEC-1 cells with the pB19-M20, pcDNA-VP1, and pcDNA-^{H153A}VP1 plasmids by Western blot analyses could be due to the presence of the transactivator activity of the B19 NS1 protein (Fig. 2B). NS1 proteins are expressed only by the pB19-M20 construct and can enhance the B19 P6 promoter activity up to 50 times in comparison to normal P6 promoter activity (33). As further demonstrated by these experiments the VP1 and ^{H153A}VP1 proteins could be detected in correct sizes. Additionally, the expression of B19-specific transcription products of the integrated VP1, ^{H153A}VP1, and VP2 constructs before and after induction with ponasterone A was analyzed by RT-PCR, which showed correct B19-specific mRNA production (data not shown).

VP1 expression accelerates Ca^{2+} entry into retinoblastoma cells. The Fura-2 fluorescence ratios (340/380 nm) in the presence of extracellular Ca^{2+} in retinoblastoma cells transfected with VP1 (1.04 ± 0.03, $n = 10$) and VP2 (1.01 ± 0.02, $n = 6$) were similar, but they were slightly higher than that in cells transfected with empty vector (0.90 ± 0.02, $n = 8$). Following stimulation of viral protein expression by ponasterone A, the fluorescence ratio was not significantly modified in cells expressing VP1 (1.01 ± 0.04, $n = 10$) or VP2 (1.00 ± 0.03, $n = 8$) or control cells transfected with the empty vector (0.91 ± 0.04, $n = 8$). Thus, ponasterone A by itself did not modify the cytosolic Ca^{2+} activity and expression of the viral proteins did not significantly alter the cytosolic Ca^{2+} activity in the presence of extracellular Ca^{2+}.

The removal of extracellular Ca^{2+} and inhibition of the vesicular Ca^{2+} pump with thapsigargin (1 μM) was followed by a rapid decrease of cytosolic Ca^{2+} activity (Fig. 3 and 4). The following addition of extracellular Ca^{2+} triggered a rapid increase of cytosolic Ca^{2+} activity (Fig. 3 and 4). Again, no significant differences were observed between cells stably transfected with VP1 or VP2. However, following treatment with ponasterone A, the Ca^{2+} entry following the readdition of extracellular Ca^{2+} was significantly more rapid in VP1-expressing cells (Fig. 3), pointing to increased activity of the Ca^{2+} release-activated Ca^{2+} channel (I_{CRAC}). In contrast, the slope of Ca^{2+} entry was not significantly modified by ponasterone A in control cells stably transfected with the empty vector (before ponasterone A treatment, 0.0077 ± 0.0012 s^{-1}, $n = 8$; after ponasterone A treatment, 0.0093 ± 0.0010 s^{-1}, $n = 8$). Similarly, Ca^{2+} entry was not significantly accelerated by the treat-

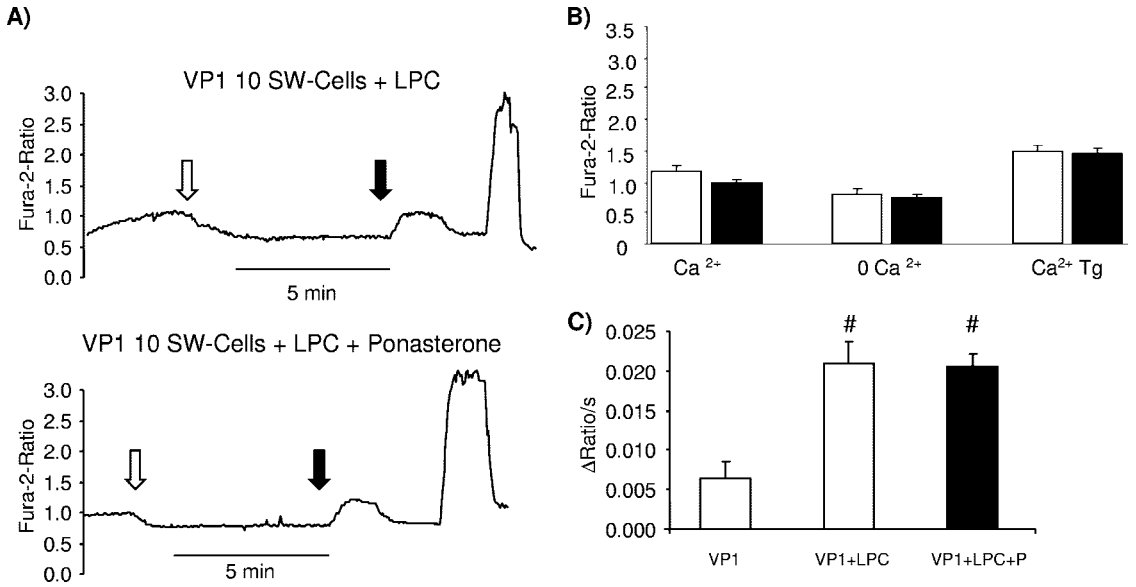

FIG. 6. Stimulation of Ca^{2+} entry by lysophosphatidylcholine. (A) Representative original tracings showing the Fura-2 fluorescence ratios (340/380 nm) in untreated (upper panel) or lysophosphatidylcholine (1 μg/ml)-treated Fura-2-loaded stably transfected VP1-expressing retinoblastoma cells (10SW) treated as described in the legend to Fig. 3. (B) Arithmetic means (± SEM; $n = 5$) of the Fura-2 fluorescence ratios after incubation as described for panel A, in Ca^{2+}-containing extracellular fluid and in Ca^{2+}-free and thapsigargin (Tg)-containing Ringer solution, and following the readdition of extracellular Ca^{2+}. Open bars represent cells in the absence of lysophosphatidylcholine, and filled bars represent cells in the presence of lysophosphatidylcholine. (C) Arithmetic means (± SEM; $n = 5$) of the slopes of increasing Fura-2 fluorescence ratios (change in ratio/second) after the readdition of Ca^{2+} in cells incubated as described for panel A, in the absence and presence of lysophosphatidylcholine (LPC). The number sign indicates a significant difference ($P \leq 0.05$, analysis of variance) compared to the respective value for cells in the absence of lysophosphatidylcholine. P, ponasterone A.

ment with ponasterone A of cells stably transfected with VP2 (Fig. 4).

The phospholipase A2-disrupting mutation ^{H153A}VP1 abrogates the acceleration of Ca^{2+} entry. The replacement of histidine by alanine in the putative phospholipase A2 catalytic subunit of VP1 (^{H153A}VP1) abolished the effect of VP1 on Ca^{2+} entry. Treatment of ^{H153A}VP1-transfected cells with ponasterone A did not significantly increase the slope of Ca^{2+} entry (Fig. 5). This observation indicates that the effect of VP1 on cellular Ca^{2+} metabolism requires the phospholipase A2 activity of the viral protein.

Stimulation of Ca^{2+} entry by lysophosphatidylcholine. When VP1-transfected cells were exposed to lysophosphatidylcholine, the slope of Ca^{2+} entry approached 0.0210 ± 0.0027 s^{-1} ($n = 5$), which was significantly higher than the value for cells in the absence of lysophosphatidylcholine (Fig. 6). Thus, the cellular effect of VP1 expression was mimicked by the phospholipase A2 product lysophosphatidylcholine (1 μg/ml). Treatment of VP1-transfected cells with ponasterone A did not further increase Ca^{2+} entry (0.0206 ± 0.0015 s^{-1}, $n = 5$), indicating that in the presence of lysophosphatidylcholine, the expression of VP1 had no additional stimulating effect on Ca^{2+} entry (Fig. 6).

Increase of Ca^{2+} entry into endothelial cells by expression of VP1. We further explored whether VP1 is similarly effective in human endothelial cells, target cells of B19 (16, 42). To this end, experiments were performed in HMEC-1 cells. The Fura-2 fluorescence ratio (340/380 nm) in the presence of extracellular Ca^{2+} in control HMEC-1 cells (0.92 ± 0.16, $n = 8$) was similar to that for VP1-expressing HMEC-1 cells (0.93 ± 0.04, $n = 8$) or ^{H153A}VP1-expressing HMEC-1 cells (1.05 ± 0.05, $n = 8$). The removal of extracellular Ca^{2+} and inhibition of the vesicular Ca^{2+} pump with thapsigargin (1 μM) was followed by a rapid decrease of cytosolic Ca^{2+} activity (Fig. 7). The slope of Ca^{2+} entry approached 0.020 ± 0.0019 s^{-1} ($n = 8$) in HMEC-1 cells with VP1, and this value was significantly higher than the value for cells in the absence of VP1 protein, 0.012 ± 0.0012 s^{-1} ($n = 8$). Replacement of histidine by alanine in the putative phospholipase A2 catalytic subunit of VP1 (^{H153A}VP1) abolished the effect of VP1 on Ca^{2+} entry while the slope of Ca^{2+} entry approached 0.014 ± 0.0013 s^{-1} ($n = 8$). Thus, similar to retinoblastoma cells, human endothelial cells respond to expression of VP1 with enhanced Ca^{2+} entry.

Increase of Ca^{2+} entry into HMEC-1 cells by transfection with full-length B19. Further studies have been performed to explore whether the replication-competent B19 plasmid (pB19-M20) was similarly able to stimulate Ca^{2+} entry. To this end, HMEC-1 cells were transfected with pB19-M20. As shown in Fig. 8, the Fura-2 ratios of fluorescence (340/380 nm) in the presence of extracellular Ca^{2+} in control HMEC-1 cells (pCR-Script) (0.80 ± 0.10, $n = 4$) and HMEC-1 cells expressing the cDNA of B19 (0.84 ± 0.06, $n = 4$) were similar.

Removal of extracellular Ca^{2+} and inhibition of the vesicular Ca^{2+} pump with thapsigargin (1 μM) resulted in a rapid decrease of cytosolic Ca^{2+} activity (Fig. 8). The following addition of extracellular Ca^{2+} triggered a rapid increase of cytosolic Ca^{2+} activity, which was significantly greater in HMEC-1 pB19-M20-transfected cells (2.59 ± 0.5199, $n = 4$) than in control HMEC-1 cells (0.89 ± 0.0277, $n = 4$). Moreover, the

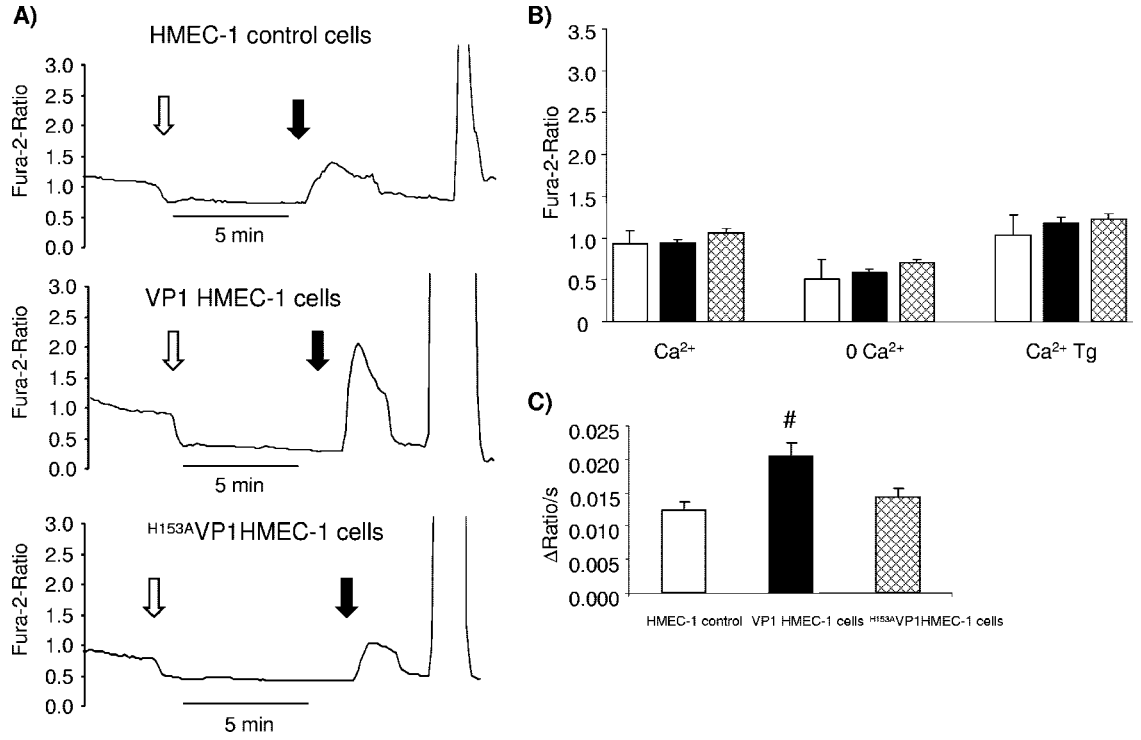

FIG. 7. Increase of Ca^{2+} entry into endothelial cells by expression of VP1. (A) Representative original tracings showing the Fura-2 fluorescence ratio (340/380 nm) in Fura-2-loaded transiently transfected endothelial cells (HMEC-1) treated as described in the legend to Fig. 3. The upper panel shows results for HMEC-1 B19-negative control cells using pCR-Script plasmid, the middle panel shows results for VP1-expressing HMEC-1 cells (VP1 HMEC-1 cells) transiently transfected with pcDNA-VP1 plasmid, and the lower panel shows ^{H153A}VP1-expressing HMEC-1 cells (^{H153A}VP1HMEC-1 cells) transiently transfected with pcDNA-^{H153A}VP1 48 h after transfection. (B) Arithmetic means (± SEM; $n = 8$) of the Fura-2 fluorescence ratios after incubation as described for panel A, in Ca^{2+}-containing extracellular fluid and in Ca^{2+}-free and thapsigargin (Tg)-containing Ringer solution, and following the readdition of extracellular Ca^{2+}. Open bars represent HMEC-1 B19-negative control cells (pCR-Script), and filled bars represent transiently transfected HMEC-1 cells with pcDNA-VP1. The cross-hatched bars represent pcDNA-^{H153A}VP1-transfected HMEC-1 cells. (C) Arithmetic means (± SEM; $n = 8$) of the slopes of increasing Fura-2 fluorescence ratios (changes in ratio/second) after the readdition of Ca^{2+} in cells incubated as described for panel A, in the HMEC-1 control vector, VP1-expressing HMEC-1 cells transiently transfected with pcDNA-VP1 plasmid (VP1 HMEC-1 cells), and ^{H153A}VP1-expressing HMEC-1 cells transiently transfected with pcDNA-^{H153A}VP1 (^{H153A}VP1HMEC-1 cells). The number sign indicates a significant difference ($P \leq 0.05$, analysis of variance) compared to the respective values for the other cells.

entry of Ca^{2+} following the readdition of extracellular Ca^{2+} was significantly more rapid in full-length B19-expressing HMEC-1 pB19-M20-transfected cells ($0.062 \pm 0.0127\ s^{-1}$, $n = 4$) than in control HMEC-1 cells ($0.019 \pm 0.0017\ s^{-1}$, $n = 4$). These observations point to enhanced stimulation of the Ca^{2+} release-activated Ca^{2+} channel (I_{CRAC}) by parvovirus B19 infection. Interestingly, the Fura-2 fluorescence ratio for entry of Ca^{2+} following the readdition of extracellular Ca^{2+} was approximately threefold higher in the presence of all viral proteins in comparison to the control, while VP1 alone increased this ratio by approximately twofold. The difference could point to some synergistic effects with other B19 proteins, such as the multifunctional NS1 protein.

DISCUSSION

Although the association between B19 infection and acute and chronic myocarditis has been established with the identification of myocardial endothelial cells as target cells (8, 16, 41, 44, 52, 82) and the role of B19 in the development of endothelial and isolated left ventricle diastolic dysfunction has been discussed (81), little is known about the pathophysiological mechanisms involved. B19 can be detected solely in endothelial cells of endomyocardial biopsy specimens of patients suffering from acute and chronic myocarditis (41). Notably, acute B19 infection may mimic ischemic disturbances of the myocardial microcirculation. The large number of endothelial cells in the close-meshed capillary and venular network of the human heart provides a reservoir for persistent as well as latent virus infection. The possible persistence of B19 infection has been demonstrated recently by the analyses of consecutive endomyocardial biopsy specimens of patients with progressive systolic left ventricle dysfunction (45, 59). With regard to the restricted B19 replication in endothelial cells, we have strong evidence that B19 RNA synthesis does occur in cardiac endothelium during acute myocarditis. A restricted B19 replication has been shown also in vitro for different cell lines (32). In order to determine possible pathophysiological mechanisms of distinct B19 proteins, we developed endothelial and nonendothelial cell culture systems, including stable inducible B19 protein-expressing cell lines. We hypothesized that the pathogenesis of B19 infection of the cardiac endothelial cells could be due to B19 proteins themselves. Along those lines, a phospho-

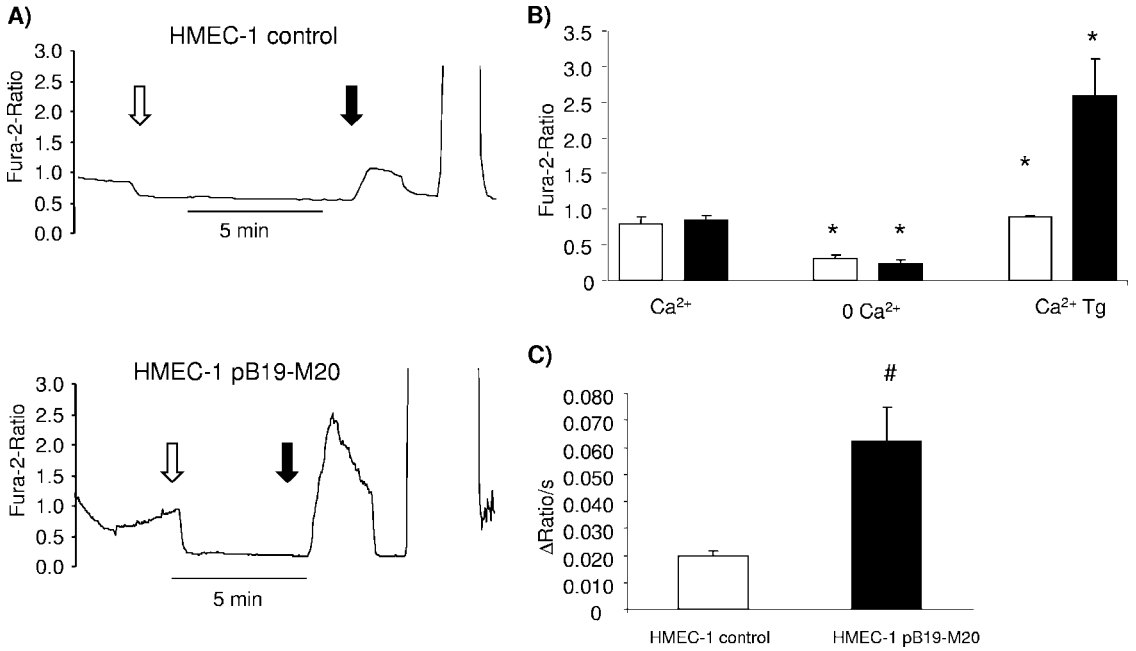

FIG. 8. Increase of Ca^{2+} entry into pB19-M20-transfected HMEC-1 cells. (A) Representative original tracings showing the Fura-2 fluorescence ratios (340/380 nm) in Fura-2-loaded HMEC-1 cells transiently transfected with the replication-competent pB19-M20 plasmid treated as described in the legend to Fig. 3. The upper panel shows results for the HMEC-1 control vector (pCR-Script), and the lower panel shows results for pB19-M20 transiently transfected HMEC-1 cells. (B) Arithmetic means (± SEM; $n = 4$) of the Fura-2 fluorescence ratios after incubation as described for panel A, in Ca^{2+}-containing extracellular fluid and in Ca^{2+}-free and thapsigargin (Tg)-containing Ringer solution, and following the readdition of extracellular Ca^{2+}. Open bars represent HMEC-1 B19-negative control cells, and filled bars represent HMEC-1 pB19-M20-transfected cells. Asterisks indicate significant difference ($P \leq 0.05$, analysis of variance) compared to the respective values for cells prior to the removal of Ca^{2+}. (C) Arithmetic means (± SEM; $n = 4$) of the slopes of increasing Fura-2 fluorescence ratios (change in ratio/second) after the readdition of Ca^{2+} as described for panel A, in the absence of the complete genome (HMEC-1 B19-negative control cells, pCR-Script) or in the presence of the complete genome (HMEC-1 pB19-M20 transfected). The number sign indicates a significant difference ($P \leq 0.05$, analysis of variance) compared to the respective value for the other cells.

lipase A2-like activity in the VP1 minor capsid protein has been identified recently (18, 26).

The present experiments disclose a novel action of parvovirus B19 on host cells. Overexpression of VP1, but not that of VP2, virtually doubles the slope of Ca^{2+} entry into Ca^{2+}-depleted cells, which is indicative of an activation of store-operated Ca^{2+} channels or Ca^{2+} release-activated Ca^{2+} channel (I_{CRAC}) (3, 62, 64). Notably, cytosolic Ca^{2+} activity is not increased during resting conditions, i.e., in the absence of I_{CRAC} activation. There was a slight variability of Fura-2 fluorescence ratios prior to the addition of ponasterone; however, this did not reach functional significance. To avoid any bias from this variability, comparisons were made between the absence and presence of ponasterone and between the absence and presence of Ca^{2+}. I_{CRAC} is not constitutively active but requires activation, which is accomplished by the depletion of cytosolic Ca^{2+} stores following the removal of extracellular Ca^{2+} and simultaneous inhibition of vesicular Ca^{2+} ATPase or by stimulation with appropriate hormones and mediators, including mitogens and inflammatory cytokines (49, 62, 89).

The present observations allow some further insight into the mechanism involved in activation of Ca^{2+} entry. The recent observation that mammalian phospholipase A2 has been shown to activate I_{CRAC} (74) prompted us to test whether the phospholipase A2 activity of VP1 accounts for the activation of Ca^{2+} entry. Thus, we abrogated the phospholipase A2 activity of VP1 by replacing a histidine with an alanine in the putative catalytic site (^{H153A}VP1). As a matter of fact, the mutation completely abolished the effect of VP1 expression on Ca^{2+} entry. Moreover, the effect of VP1 expression was mimicked by the addition of lysophosphatidylcholine, a product of phospholipase A2. As discussed earlier (74), arachidonic acid appears not to be involved in activation of I_{CRAC}. Whatever product is involved, it appears safe to conclude that VP1 affects Ca^{2+} entry by virtue of its phospholipase A2 activity.

The pleiotropic actions of phospholipase A2 (73, 84) include the stimulation of smooth muscle and endothelial cells (22, 72). Altered regulation of cytosolic Ca^{2+} activity is expected to affect a wide variety of cellular functions. Ca^{2+} is involved in the control of exocytosis, contraction, enzyme activity, and gene expression (4–6, 62). As reviewed elsewhere (46), cytosolic Ca^{2+} activity further plays a critical role in the regulation of cell proliferation (4–6, 62, 69, 70, 83). I_{CRAC} is stimulated by growth factors (65) and triggers Ca^{2+} entry and subsequent Ca^{2+} oscillations into proliferating cells (47), an effect required for stimulation of cell proliferation (46). Conversely, lymphocyte apoptosis following CD95 receptor triggering is paralleled by the inhibition of I_{CRAC} (23, 49). The inhibition of I_{CRAC} abrogates activation and proliferation of lymphocytes (23, 49). It is tempting to speculate that the stimulation of I_{CRAC} serves to stimulate proliferation of the infected cell, which may foster viral replication (79). We hypothesize that

the demonstrated B19 phospholipase A2 activity upon Ca^{2+} entry may be a consequence of early B19 infection steps. The hypothesis is strongly supported by the observation that the B19 phospholipase A2 activity on the viral capsid plays a key role in synoviocyte activation (51). Along those lines, VP1 polypeptides and VP1 domains sticking out from partially degraded capsids may be subject to different regulatory properties during the B19 infection cycle (40, 51, 67, 68). On the other hand, our in vitro results presented here also indicate that the VP1 PLA2 activity on the regulation of Ca^{2+} entry may be effective after protein synthesis, as shown by the experiments using the pB19-M20 full-length clone. The fact that B19 replication depends on proliferative active cells and that altered cytosolic Ca^{2+} activity supports cell proliferation which can foster viral replication point to viral PLA2 activity of invading viruses to stimulate endothelial cell proliferation. In contrast to expression of VP1 or VP2, however, expression of B19 protein NS1 triggers apoptosis, an effect apparently involving mechanisms other than Ca^{2+} entry (66).

In conclusion, the present observations indicate that the parvoviral B19 protein VP1 leads to activation of I_{CRAC}, an effect likely participating in the pathophysiology of parvovirus B19 infection.

ACKNOWLEDGMENTS

We acknowledge the technical assistance of E. Faber and the meticulous preparation of the manuscript by Lejla Subasic and Tanja Loch.

This study was supported by the Deutsche Forschungsgemeinschaft, SFB-Transregio 19 (project TP B5), the Bundesministerium für Bildung, Wissenschaft, Forschung und Technologie (Center for Interdisciplinary Clinical Research) (grant 01 KS 9602), and the Karl-Kuhn Stiftung to C.-T.B.

REFERENCES

1. **Anderson, M. J., S. E. Jones, S. P. Fisher-Hoch, E. Lewis, S. M. Hall, C. L. Bartlett, B. J. Cohen, P. P. Mortimer, and M. S. Pereira.** 1983. Human parvovirus, the cause of erythema infectiosum (fifth disease)? Lancet **i:**1378.
2. **Barah, F., P. J. Vallely, M. L. Chiswick, G. M. Cleator, and J. R. Kerr.** 2001. Association of human parvovirus B19 infection with acute meningoencephalitis. Lancet **358:**729–730.
3. **Berridge, M. J.** 1995. Capacitative calcium entry. Biochem. J. **312:**1–11.
4. **Berridge, M. J., M. D. Bootman, and P. Lipp.** 1998. Calcium—a life and death signal. Nature **395:**645–648.
5. **Berridge, M. J., M. D. Bootman, and H. L. Roderick.** 2003. Calcium signalling: dynamics, homeostasis and remodelling. Nat Rev. Mol. Cell Biol. **4:**517–529.
6. **Berridge, M. J., P. Lipp, and M. D. Bootman.** 2000. The versatility and universality of calcium signalling. Nat. Rev. Mol. Cell Biol. **1:**11–21.
7. **Bock, C. T.** 2006. Parvovirus B19: a new emerging pathogenic agent of inflammatory cardiomyopathy. Ernst Schering Res. Found. Workshop **2006:** 83–97.
8. **Bock, C. T., K. Klingel, S. Aberle, A. Duechting, A. Lupescu, F. Lang, and R. Kandolf.** 2005. Human parvovirus B19: a new emerging pathogen of inflammatory cardiomyopathy. J. Vet. Med. B **52:**340–343.
9. **Bock, C. T., H. L. Tillmann, H. J. Maschek, M. P. Manns, and C. Trautwein.** 1997. A preS mutation isolated from a patient with chronic hepatitis B infection leads to virus retention and misassembly. Gastroenterology **113:** 1976–1982.
10. **Brown, K. E.** 1989. What threat is human parvovirus B19 to the fetus? Br. J. Obstet. Gynaecol. **96:**764–767.
11. **Brown, K. E.** 2004. Variants of B19. Dev. Biol. (Basel) **118:**71–77.
12. **Brown, K. E., S. M. Anderson, and N. S. Young.** 1993. Erythrocyte P antigen: cellular receptor for B19 parvovirus. Science **262:**114–117.
13. **Brown, K. E., J. R. Hibbs, G. Gallinella, S. M. Anderson, E. D. Lehman, P. McCarthy, and N. S. Young.** 1994. Resistance to parvovirus B19 infection due to lack of virus receptor (erythrocyte P antigen). N. Engl. J. Med. **330:**1192–1196.
14. **Brown, K. E., Z. Liu, G. Gallinella, S. Wong, I. P. Mills, and M. G. O'Sullivan.** 2004. Simian parvovirus infection: a potential zoonosis. J Infect. Dis. **190:**1900–1907.
15. **Brown, K. E., N. S. Young, and J. M. Liu.** 1994. Molecular, cellular and clinical aspects of parvovirus B19 infection. Crit. Rev. Oncol. Hematol. **16:**1–31.
16. **Bultmann, B. D., K. Klingel, K. Sotlar, C. T. Bock, H. A. Baba, M. Sauter, and R. Kandolf.** 2003. Fatal parvovirus B19-associated myocarditis clinically mimicking ischemic heart disease: an endothelial cell-mediated disease. Hum. Pathol. **34:**92–95.
17. **Bultmann, B. D., K. Sotlar, and K. Klingel.** 2004. Parvovirus B19. N. Engl. J. Med. **350:**2006–2007.
18. **Canaan, S., Z. Zadori, F. Ghomashchi, J. Bollinger, M. Sadilek, M. E. Moreau, P. Tijssen, and M. H. Gelb.** 2004. Interfacial enzymology of parvovirus phospholipases A2. J. Biol. Chem. **279:**14502–14508.
19. **Corman, L. C., and D. J. Dolson.** 1992. Polyarteritis nodosa and parvovirus B19 infection. Lancet **339:**491.
20. **Cotmore, S. F., V. C. McKie, L. J. Anderson, C. R. Astell, and P. Tattersall.** 1986. Identification of the major structural and nonstructural proteins encoded by human parvovirus B19 and mapping of their genes by procaryotic expression of isolated genomic fragments. J. Virol. **60:**548–557.
21. **Crane, J.** 2002. Parvovirus B19 infection in pregnancy. J. Obstet. Gynaecol. Can. **24:**727–743.
22. **Creer, M. H., and J. McHowat.** 1998. Selective hydrolysis of plasmalogens in endothelial cells following thrombin stimulation. Am. J. Physiol. **275:**C1498–C1507.
23. **Dangel, G. R., F. Lang, and A. Lepple-Wienhues.** 2005. Effect of sphingosine on Ca^{2+} entry and mitochondrial potential of Jurkat T cells—interaction with Bcl2. Cell. Physiol. Biochem. **16:**9–14.
24. **Dingli, D., D. H. Pfizenmaier, E. Arromdee, P. Wennberg, P. C. Spittell, A. Chang-Miller, and B. L. Clarke.** 2000. Severe digital arterial occlusive disease and acute parvovirus B19 infection. Lancet **356:**312–314.
25. **Doerig, C., P. Beard, and B. Hirt.** 1987. A transcriptional promoter of the human parvovirus B19 active in vitro and in vivo. Virology **157:**539–542.
26. **Dorsch, S., G. Liebisch, B. Kaufmann, P. von Landenberg, J. H. Hoffmann, W. Drobnik, and S. Modrow.** 2002. The VP1 unique region of parvovirus B19 and its constituent phospholipase A2-like activity. J. Virol. **76:**2014–2018.
27. **Drago, F., M. Semino, P. Rampini, and A. Rebora.** 1999. Parvovirus B19 infection associated with acute hepatitis and a purpuric exanthem. Br. J. Dermatol. **141:**160–161.
28. **Ellis, R. J., M. E. Childers, M. Cherner, D. Lazzaretto, S. Letendre, and I. Grant.** 2003. Increased human immunodeficiency virus loads in active methamphetamine users are explained by reduced effectiveness of antiretroviral therapy. J. Infect. Dis. **188:**1820–1826.
29. **Ellis, R. J., M. E. Childers, J. D. Zimmerman, S. D. Frost, R. Deutsch, and J. A. McCutchan.** 2003. Human immunodeficiency virus-1 RNA levels in cerebrospinal fluid exhibit a set point in clinically stable patients not receiving antiretroviral therapy. J. Infect. Dis. **187:**1818–1821.
30. **Enders, G., J. Dotsch, J. Bauer, W. Nutzenadel, H. Hengel, D. Haffner, G. Schalasta, K. Searle, and K. E. Brown.** 1998. Life-threatening parvovirus B19-associated myocarditis and cardiac transplantation as possible therapy: two case reports. Clin. Infect. Dis. **26:**355–358.
31. **Finkel, T. H., T. J. Torok, P. J. Ferguson, E. L. Durigon, S. R. Zaki, D. Y. Leung, R. J. Harbeck, E. W. Gelfand, F. T. Saulsbury, J. R. Hollister, et al.** 1994. Chronic parvovirus B19 infection and systemic necrotising vasculitis: opportunistic infection or aetiological agent? Lancet **343:**1255–1258.
32. **Gallinella, G., E. Manaresi, E. Zuffi, S. Venturoli, L. Bonsi, G. P. Bagnara, M. Musiani, and M. Zerbini.** 2000. Different patterns of restriction to B19 parvovirus replication in human blast cell lines. Virology **278:**361–367.
33. **Gareus, R., A. Gigler, A. Hemauer, M. Leruez-Ville, F. Morinet, H. Wolf, and S. Modrow.** 1998. Characterization of cis-acting and NS1 protein-responsive elements in the p6 promoter of parvovirus B19. J. Virol. **72:**609–616.
34. **Gigler, A., S. Dorsch, A. Hemauer, C. Williams, S. Kim, N. S. Young, S. Zolla-Pazner, H. Wolf, M. K. Gorny, and S. Modrow.** 1999. Generation of neutralizing human monoclonal antibodies against parvovirus B19 proteins. J. Virol. **73:**1974–1979.
35. **Heegaard, E. D., and K. E. Brown.** 2002. Human parvovirus B19. Clin. Microbiol. Rev. **15:**485–505.
36. **Hillingso, J. G., I. P. Jensen, and L. Tom-Petersen.** 1998. Parvovirus B19 and acute hepatitis in adults. Lancet **351:**955–956.
37. **Hsu, T. C., W. J. Wu, M. C. Chen, and G. J. Tsay.** 2004. Human parvovirus B19 non-structural protein (NS1) induces apoptosis through mitochondria cell death pathway in COS-7 cells. Scand. J. Infect. Dis. **36:**570–577.
38. **Karetnyi, Y. V., P. R. Beck, R. S. Markin, A. N. Langnas, and S. J. Naides.** 1999. Human parvovirus B19 infection in acute fulminant liver failure. Arch. Virol. **144:**1713–1724.
39. **Katz, V. L., N. C. Chescheir, and M. Bethea.** 1990. Hydrops fetalis from B19 parvovirus infection. J. Perinatol. **10:**366–368.
40. **Kawase, M., M. Momoeda, N. S. Young, and S. Kajigaya.** 1995. Most of the VP1 unique region of B19 parvovirus is on the capsid surface. Virology **211:**359–366.
41. **Klingel, K., H.-C. Selinka, M. Sauter, C.-T. Bock, G. Szalay, and R. Kandolf.** 2002. Molecular mechanisms in enterovirus and parvovirus B19 associated myocarditis and inflammatory cardiomyopathy. Eur. Heart J. Suppl. **4**(Suppl. I)**:**I8–I12.

42. **Klingel, K., M. Sauter, C. T. Bock, G. Szalay, J. J. Schnorr, and R. Kandolf.** 2004. Molecular pathology of inflammatory cardiomyopathy. Med. Microbiol. Immunol. (Berlin) **193:**101–107.
43. **Koch, W. C.** 2001. Fifth (human parvovirus) and sixth (herpesvirus 6) diseases. Curr. Opin. Infect. Dis. **14:**343–356.
44. **Kuhl, U., M. Pauschinger, T. Bock, K. Klingel, C. P. Schwimmbeck, B. Seeberg, L. Krautwurm, W. Poller, H. P. Schultheiss, and R. Kandolf.** 2003. Parvovirus B19 infection mimicking acute myocardial infarction. Circulation **108:**945–950.
45. **Kuhl, U., M. Pauschinger, B. Seeberg, D. Lassner, M. Noutsias, W. Poller, and H. P. Schultheiss.** 2005. Viral persistence in the myocardium is associated with progressive cardiac dysfunction. Circulation **112:**1965–1970.
46. **Lang, F., M. Foeller, K. S. Lang, P. A. Lang, M. Ritter, E. Gulbins, A. Vereninov, and S. M. Huber.** 2005. Ion channels in cell proliferation and apoptotic cell death. J. Membr. Biol. **205:**147–157.
47. **Lang, F., F. Friedrich, E. Kahn, E. Woll, M. Hammerer, S. Waldegger, K. Maly, and H. Grunicke.** 1991. Bradykinin-induced oscillations of cell membrane potential in cells expressing the Ha-ras oncogene. J. Biol. Chem. **266:**4938–4942.
48. **Lehmann, H. W., A. Knoll, R. M. Kuster, and S. Modrow.** 2003. Frequent infection with a viral pathogen, parvovirus B19, in rheumatic diseases of childhood. Arthritis Rheum. **48:**1631–1638.
49. **Lepple-Wienhues, A., C. Belka, T. Laun, A. Jekle, B. Walter, U. Wieland, M. Welz, L. Heil, J. Kun, G. Busch, M. Weller, M. Bamberg, E. Gulbins, and F. Lang.** 1999. Stimulation of CD95 (Fas) blocks T lymphocyte calcium channels through sphingomyelinase and sphingolipids. Proc. Natl. Acad. Sci. USA **96:**13795–13800.
50. **Li, Y., Z. Zadori, H. Bando, R. Dubuc, G. Fediere, J. Szelei, and P. Tijssen.** 2001. Genome organization of the densovirus from Bombyx mori (BmDNV-1) and enzyme activity of its capsid. J. Gen. Virol. **82:**2821–2825.
51. **Lu, J., N. Zhi, S. Wong, and K. E. Brown.** 2006. Activation of synoviocytes by the secreted phospholipase A2 motif in the VP1-unique region of parvovirus B19 minor capsid protein. J. Infect. Dis. **193:**582–590.
52. **Magro, C. M., G. Nuovo, C. Ferri, A. N. Crowson, D. Giuggioli, and M. Sebastiani.** 2004. Parvoviral infection of endothelial cells and stromal fibroblasts: a possible pathogenetic role in scleroderma. J. Cutan. Pathol. **31:**43–50.
53. **Malm, C., E. Fridell, and K. Jansson.** 1993. Heart failure after parvovirus B19 infection. Lancet **341:**1408–1409.
54. **Mitchell, L. A.** 2002. Parvovirus B19 nonstructural (NS1) protein as a transactivator of interleukin-6 synthesis: common pathway in inflammatory sequelae of human parvovirus infections? J. Med. Virol. **67:**267–274.
55. **Moffatt, S., N. Yaegashi, K. Tada, N. Tanaka, and K. Sugamura.** 1998. Human parvovirus B19 nonstructural (NS1) protein induces apoptosis in erythroid lineage cells. J. Virol. **72:**3018–3028.
56. **Moore, T. L.** 2000. Parvovirus-associated arthritis. Curr. Opin. Rheumatol. **12:**289–294.
57. **Munakata, Y., T. Saito-Ito, K. Kumura-Ishii, J. Huang, T. Kodera, T. Ishii, Y. Hirabayashi, Y. Koyanagi, and T. Sasaki.** 2005. Ku80 autoantigen as a cellular coreceptor for human parvovirus B19 infection. Blood **106:**3449–3456.
58. **Murry, C. E., K. R. Jerome, and D. D. Reichenbach.** 2001. Fatal parvovirus myocarditis in a 5-year-old girl. Hum. Pathol. **32:**342–345.
59. **Nigro, G., V. Bastianon, V. Colloridi, F. Ventriglia, P. Gallo, G. D'Amati, W. C. Koch, and S. P. Adler.** 2000. Human parvovirus B19 infection in infancy associated with acute and chronic lymphocytic myocarditis and high cytokine levels: report of 3 cases and review. Clin. Infect. Dis. **31:**65–69.
60. **Orth, T., W. Herr, T. Spahn, T. Voigtlander, D. Michel, T. Mertens, W. J. Mayet, W. Dippold, and K. H. Meyer zum Buschenfelde.** 1997. Human parvovirus B19 infection associated with severe acute perimyocarditis in a 34-year-old man. Eur. Heart J. **18:**524–525.
61. **Oyer, C. E., E. H. Ongcapin, J. Ni, N. E. Bowles, and J. A. Towbin.** 2000. Fatal intrauterine adenoviral endomyocarditis with aortic and pulmonary valve stenosis: diagnosis by polymerase chain reaction. Hum. Pathol. **31:**1433–1435.
62. **Parekh, A. B., and R. Penner.** 1997. Store depletion and calcium influx. Physiol. Rev. **77:**901–930.
63. **Pattison, J. R.** 1988. Diseases caused by the human parvovirus B19. Arch. Dis. Child. **63:**1426–1427.
64. **Putney, J. W., Jr., and G. S. Bird.** 1993. The signal for capacitative calcium entry. Cell **75:**199–201.
65. **Qian, D., and A. Weiss.** 1997. T cell antigen receptor signal transduction. Curr. Opin. Cell Biol. **9:**205–212.
66. **Raab, U., K. Beckenlehner, T. Lowin, H. H. Niller, S. Doyle, and S. Modrow.** 2002. NS1 protein of parvovirus B19 interacts directly with DNA sequences of the p6 promoter and with the cellular transcription factors Sp1/Sp3. Virology **293:**86–93.
67. **Rosenfeld, S. J., K. Yoshimoto, S. Kajigaya, S. Anderson, N. S. Young, A. Field, P. Warrener, G. Bansal, and M. S. Collett.** 1992. Unique region of the minor capsid protein of human parvovirus B19 is exposed on the virion surface. J. Clin. Investig. **89:**2023–2029.
68. **Saikawa, T., S. Anderson, M. Momoeda, S. Kajigaya, and N. S. Young.** 1993. Neutralizing linear epitopes of B19 parvovirus cluster in the VP1 unique and VP1-VP2 junction regions. J. Virol. **67:**3004–3009.
69. **Santella, L.** 1998. The role of calcium in the cell cycle: facts and hypotheses. Biochem. Biophys. Res. Commun. **244:**317–324.
70. **Santella, L., K. Kyozuka, L. De Riso, and E. Carafoli.** 1998. Calcium, protease action, and the regulation of the cell cycle. Cell Calcium **23:**123–130.
71. **Schowengerdt, K. O., J. Ni, S. W. Denfield, R. J. Gajarski, N. E. Bowles, G. Rosenthal, D. L. Kearney, J. K. Price, B. B. Rogers, G. M. Schauer, R. E. Chinnock, and J. A. Towbin.** 1997. Association of parvovirus B19 genome in children with myocarditis and cardiac allograft rejection: diagnosis using the polymerase chain reaction. Circulation **96:**3549–3554.
72. **Seegers, H. C., R. W. Gross, and W. A. Boyle.** 2002. Calcium-independent phospholipase A(2)-derived arachidonic acid is essential for endothelium-dependent relaxation by acetylcholine. J. Pharmacol. Exp. Ther. **302:**918–923.
73. **Six, D. A., and E. A. Dennis.** 2000. The expanding superfamily of phospholipase A(2) enzymes: classification and characterization. Biochim. Biophys. Acta **1488:**1–19.
74. **Smani, T., S. I. Zakharov, E. Leno, P. Csutora, E. S. Trepakova, and V. M. Bolotina.** 2003. Ca^{2+}-independent phospholipase A2 is a novel determinant of store-operated Ca^{2+} entry. J. Biol. Chem. **278:**11909–11915.
75. **Sokal, E. M., M. Melchior, C. Cornu, A. T. Vandenbroucke, J. P. Buts, B. J. Cohen, and G. Burtonboy.** 1998. Acute parvovirus B19 infection associated with fulminant hepatitis of favourable prognosis in young children. Lancet **352:**1739–1741.
76. **Sol, N., J. Le Junter, I. Vassias, J. M. Freyssinier, A. Thomas, A. F. Prigent, B. B. Rudkin, S. Fichelson, and F. Morinet.** 1999. Possible interactions between the NS-1 protein and tumor necrosis factor alpha pathways in erythroid cell apoptosis induced by human parvovirus B19. J. Virol. **73:**8762–8770.
77. **Takahashi, Y., C. Murai, S. Shibata, Y. Munakata, T. Ishii, K. Ishii, T. Saitoh, T. Sawai, K. Sugamura, and T. Sasaki.** 1998. Human parvovirus B19 as a causative agent for rheumatoid arthritis. Proc. Natl. Acad. Sci. USA **95:**8227–8232.
78. **Tanneur, V., D. Ilgaz, C. Duranton, S. Fillon, N. Gamper, S. M. Huber, and F. Lang.** 2002. Time-dependent regulation of capacitative Ca^{2+} entry by IGF-1 in human embryonic kidney cells. Pflugers Arch. **445:**74–79.
79. **Teleman, A., M. Tuynder, T. Dupressoir, B. Robaye, F. Sigaux, E. Shaulian, M. Oren, J. Rommelaere, and R. Amson.** 1993. A model for tumor suppression using H-1 parvovirus. Proc. Natl. Acad. Sci. USA **90:**8702–8706.
80. **Trapani, S., M. Ermini, and F. Falcini.** 1999. Human parvovirus B19 infection: its relationship with systemic lupus erythematosus. Semin. Arthritis Rheum. **28:**319–325.
81. **Tschope, C., C. T. Bock, M. Kasner, M. Noutsias, D. Westermann, P. L. Schwimmbeck, M. Pauschinger, W. C. Poller, U. Kuhl, R. Kandolf, and H. P. Schultheiss.** 2005. High prevalence of cardiac parvovirus B19 infection in patients with isolated left ventricular diastolic dysfunction. Circulation **111:**879–886.
82. **Weigel-Kelley, K. A., M. C. Yoder, and A. Srivastava.** 2003. Alpha5beta1 integrin as a cellular coreceptor for human parvovirus B19: requirement of functional activation of beta1 integrin for viral entry. Blood **102:**3927–3933.
83. **Whitfield, J. F., R. P. Bird, B. R. Chakravarthy, R. J. Isaacs, and P. Morley.** 1995. Calcium-cell cycle regulator, differentiator, killer, chemopreventor, and maybe, tumor promoter. J. Cell. Biochem. Suppl. **22:**74–91.
84. **Winstead, M. V., J. Balsinde, and E. A. Dennis.** 2000. Calcium-independent phospholipase A(2): structure and function. Biochim. Biophys. Acta **1488:**28–39.
85. **Yoto, Y., T. Kudoh, K. Haseyama, N. Suzuki, and S. Chiba.** 1996. Human parvovirus B19 infection associated with acute hepatitis. Lancet **347:**868–869.
86. **Young, N. S., and K. E. Brown.** 2004. Parvovirus B19. N. Engl. J. Med. **350:**586–597.
87. **Zadori, Z., J. Szelei, M. C. Lacoste, Y. Li, S. Gariepy, P. Raymond, M. Allaire, I. R. Nabi, and P. Tijssen.** 2001. A viral phospholipase A2 is required for parvovirus infectivity. Dev. Cell **1:**291–302.
88. **Zhi, N., Z. Zadori, K. E. Brown, and P. Tijssen.** 2004. Construction and sequencing of an infectious clone of the human parvovirus B19. Virology **318:**142–152.
89. **Zweifach, A., and R. S. Lewis.** 1993. Mitogen-regulated Ca^{2+} current of T lymphocytes is activated by depletion of intracellular Ca^{2+} stores. Proc. Natl. Acad. Sci. USA **90:**6295–6299.